



University of Dundee

On solitary wave breaking and impact on a horizontal deck

Liu, Jiaqi; Hayatdavoodi, Masoud

DOI:
[10.3390/jmse11051033](https://doi.org/10.3390/jmse11051033)

Publication date:
2023

Licence:
CC BY

Document Version
Publisher's PDF, also known as Version of record

[Link to publication in Discovery Research Portal](#)

Citation for published version (APA):
Liu, J., & Hayatdavoodi, M. (2023). On solitary wave breaking and impact on a horizontal deck. *Journal of Marine Science and Engineering*, 11(5), [1033]. <https://doi.org/10.3390/jmse11051033>

General rights

Copyright and moral rights for the publications made accessible in Discovery Research Portal are retained by the authors and/or other copyright owners and it is a condition of accessing publications that users recognise and abide by the legal requirements associated with these rights.


- Users may download and print one copy of any publication from Discovery Research Portal for the purpose of private study or research.
- You may not further distribute the material or use it for any profit-making activity or commercial gain.
- You may freely distribute the URL identifying the publication in the public portal.

Take down policy

If you believe that this document breaches copyright please contact us providing details, and we will remove access to the work immediately and investigate your claim.

Article

On Solitary Wave Breaking and Impact on a Horizontal Deck

Jiaqi Liu ^{1,*} and Masoud Hayatdavoodi ^{1,2} 

¹ College of Shipbuilding Engineering, Harbin Engineering University, Harbin 150001, China

² Civil Engineering Department, School of Science and Engineering, University of Dundee, Dundee DD1 4HN, UK

* Correspondence: jiaqi_liu@hrbeu.edu.cn; Tel.: +86-195-2633-7709

Abstract: The impact of waves and bores generated by broken solitary waves on horizontal decks of coastal structures was studied by solving the Navier–Stokes equations. Solitary waves of different amplitudes were considered, and submerged ramps were used to bring the waves to the breaking point. The horizontal fixed deck was located downwave of the ramp and placed at various elevations above and below the still-water level. The results include the surface elevation of the wave and the bore-induced horizontal and vertical forces on the deck. The results were compared with laboratory measurements and those due to the bore generated by breaking a reservoir, and a discussion is provided on the relative magnitude of the loads. It is found that breaking solitary waves and dam-break provide reasonable loading conclusions for tsunamis events.

Keywords: bore generation; solitary wave breaking; bore loads; horizontal deck

1. Introduction

Tsunamis, oceanic waves with small amplitudes (usually less than 1 m) in deep water and long wavelengths (usually hundreds of kilometers), are generated by the rapid displacement of water mainly due to earthquakes, underwater landslides, and volcanic eruptions. In shallow areas or dry lands, tsunami waves break into a number of solitons and usually form a turbulent bore; see [1–4]. A train of breaking waves and bore are formed, impacting coastal structures. Significant damage has been caused by tsunamis' impact on coastal structures, especially coastal bridges. In particular, the failure of coastal bridges significantly impacts the transportation system, given that the connections to the disaster-affected areas are cut off. This may result in a delayed rescue and recovery of areas affected by the destructive events.

In the failure of a bridge, a body of fluid, i.e., wave or bore, impacts the bridge, resulting in loads larger than the bridge's capacity. In almost every major oceanic event in the past few decades, coastal bridge failures have been observed. The tsunami caused by the 2004 Sumatra earthquake impacted hundreds of bridges on the west coast of Sumatra, Indonesia; see [5]. More than 250 coastal bridges were damaged by the 2011 Tōhoku tsunamis; see [6]. Studies on the bore impact on bridges are traditionally divided into two categories, namely (i) the generation of a tsunami-like bore by using solitary waves, breaking solitary waves, and breaking the dam of a reservoir (namely dam-break), and (ii) bore impact on the bridge. Both of them were studied in this work.

In most tsunami events, tsunamis are caused by earthquakes. Many bridges can survive the earthquake but fail to resist the impact of tsunamis; see [7]. In these failures, the bridge pipes remain whereas the bridge deck collapses. The impact of fluid on the bridge deck can be subdivided into horizontal and vertical force. If the peak value of vertical force equals or exceeds the vertical resistance of the connection part between the bridge deck and pipes, even a small horizontal force could push the deck off, or failure happens directly due to the large peak value of horizontal force. Hence, strengthening the resistance of the connections is suggested to reduce this kind of failure, where the wave–structure interaction



Citation: Liu, J.; Hayatdavoodi, M. On Solitary Wave Breaking and Impact on a Horizontal Deck. *J. Mar. Sci. Eng.* **2023**, *11*, 1033. <https://doi.org/10.3390/jmse11051033>

Academic Editor: Jens Engström

Received: 10 March 2023

Revised: 5 May 2023

Accepted: 8 May 2023

Published: 12 May 2023



Copyright: © 2023 by the authors. Licensee MDPI, Basel, Switzerland. This article is an open access article distributed under the terms and conditions of the Creative Commons Attribution (CC BY) license (<https://creativecommons.org/licenses/by/4.0/>).

is considered. On the other hand, failure still happens when the tsunami-induced impact is too large, even if the connection was designed to be strong enough according to the industrial standard; see [7]. To this extent, the generation mechanism of a tsunami-like bore directly affects the profile, propagation speed, and flow field. The peak value of the wave–structure interaction of a tsunami-induced bore is suggested to be studied.

When a tsunami approaches the shore, its wave speed decreases according to $c = \sqrt{gh}$ in shallow water, where c is the wave speed, g is the gravitational acceleration, and h is the water depth, and its skewness, asymmetry, and wave height increase; see [3,8]. On dry lands and shallow areas, tsunami waves usually form a turbulent bore, and the effects of frequency dispersion balance non-linearity, while some certain huge waves break directly; see [1–4]. The un-breaking waves transform into a bore. As the formed bore shoaling, a train of breaking waves is formed, impacting the coastal and adjacent structures. Due to the instantaneity of the occurrence of a tsunami, there is little record about the Grimshaw-derived [9] equations used to describe the amplitudes of solitary waves with slowly varied floors by energy conservation. Benilov et al. [10] related the amplitude and velocity of an envelope soliton (packet of surface gravity waves or a series of solitary) to the depth in the topography-modified Schrödinger equation. They reported that the amplitude of a shoaling soliton decreases as it propagates. Grimshaw and Annenkov [11] used a higher-order nonlinear Schrödinger equation to describe the deformation of a soliton. In their equation, the soliton can penetrate a shallow depth smaller than $\frac{1.363m}{\text{wave number}}$. Rajan et al. [12] used the Djordjević and Redekopp equation—see [13]—to study a soliton. The maximum amplitude of the soliton decreases or increases as the water depth decreases or increases. Nik et al. [14] used the Korteweg–de Vries (KdV) equation—see [15]—to study the internal solitary wave propagating on variable topography, such as a constant-slope bottom and specific bottom profile following the previous studies. A secondary trailing wave packet was found after the wave passes the topographies. Wang et al. [16] carried out laboratorial experiments to study O-solitons (solitary waves whose crest is shaped like the letter “o”). The phase of this kind of solitary wave remains after the collapse for a short period. Quezada and Ketcheson [17] derived a KdV-type equation to study the propagations of solitary waves over a periodically varied bottom. The effective dispersion of solitary waves on the bottom was reported in detail. According to these studies, the breaking method of a solitary wave could usually be the bottom variation, such as a gentle slope.

Many experiments have been conducted to study the impact on deck. Bradner et al. [18] conducted experiments to study the wave forces on causeway-type coastal highway bridges using a wide range of regular and random wave conditions. In order to gain an insight into the tsunami forces that various types of bridges have to withstand, ref. [19] conducted experiments to test the tsunami bore impact on 1:20-scale bridge specimens with different shapes. A series of laboratory experiments and CFD calculations were conducted by [20] to study the horizontal and vertical forces of solitary waves on a horizontal plate. Istrati et al. [21] conducted the largest experiments, on a 1:5 scale, of a tsunami impact on a straight single-span bridge. The total forces on the bridge and the distribution in individual bearing connections were reported. Xiang et al. [22] employed a solitary wave to represent a tsunami. The horizontal and vertical fluid impact forces on a bridge superstructure, on a 1:5 scale, were studied through large-scale laboratory experiments and numerical simulations. Istrati and Buckle [23] conducted the largest-scale experiments of tsunami impact on an open-girder skewed bridge specimen with a 45° angle.

For the analytical simulations of the impact on deck, ref. [24] investigated the interaction between a train of surface gravity wave and a horizontal plate by assuming that the wavelength and plate length are more significant than the water depth. An analytical solution was provided under that assumption. Hayatdavoodi et al. [25] studied the horizontal and vertical wave forces of cnoidal waves on a horizontal flat plate in shallow water. Based on Level I Green–Naghdi equations, a nonlinear shallow-water model was provided to study and compare with laboratorial experimental data.

Two main types of mesh are used in the computational simulations based on the Navier–Stokes equations. One type is the mesh-based method. Azadbakht [26] conducted a 2D numerical simulation of tsunami impact on simplified models of bridges located on the West Coast of the US by using finite element models. Istratiand and Buckle [27] investigated, via 2D and more realistic 3D CFD modeling, the tsunami impact on prototype box-girder bridges located in Oregon, US, and developed appropriate design procedures that were included in the first tsunami design guidelines developed in the US. Hayatdavoodi and Ertekin [28] and Hayatdavoodi et al. [29] employed the Navier–Stokes equations and Green–Naghdi equations to study the solitary wave impact on a horizontal deck. The second type is the particle-based method. Mohammad and Ali [30] used the smoothed particle hydrodynamics (SPHs) method to investigate the tsunami wave loads on bridge decks. Hasanpour et al. [31] used the SPHs method to study the impact of tsunami debris on bridge decks.

For the generation mechanism of a tsunami-like bore, a solitary wave has been frequently used to study tsunamis (see [32–35]) at their beginning. However, these studies do not explain why solitary waves or cnoidal waves are used to study tsunamis, as pointed out by [3]. Many observations and much research suggest that the length and profile of tsunamis are different from those of solitary waves (see [3,36]). Moreover, most coastal structures are near or after the shore, where the waves become bores. The phenomenon of the disintegration of long waves into shorter waves has been observed in many tsunami events, such as the Indian Ocean tsunami in 2004, when the tsunami approached the shore; see [37]. When the wavefront becomes sufficiently steep due to the change in water depth, it breaks into small waves and an undular bore. Hence, a dam-break-generated bore is employed as a tsunami-like bore in many tsunami studies (see [38,39]).

Madsen et al. [3] investigated the propagation of a tsunami by considering a symmetric smooth wave propagating over a gentle ramp, which could induce the breaking of the wave. The conclusion is that the breaking has an additional effect, where the breaking happens, on bore impact on coastal structures. Some researchers have studied the solitary wave break during the propagation over a ramp and studied the impact on the structure in their studies, e.g., [40]. Manoochehr et al. [41] carried out laboratorial experiments to study the solitary breaking wave impact, where a solitary wave passes over a ramp with different coastal slopes, breaks, and propagates on a flat platform. The selection of the coastal slopes is due to the slope range tested by [42]. Istrati [43] broke the solitary wave with a ramp, whose slope is 1:12, in their large wave flume to study the impact on the box-girder. The onset of the breaking point and the location of the bore formation were identified. Yang et al. [44] broke the solitary wave in the same way by a fixed slope to study the impact on a box-girder bridge. Neither of them discussed the relationship between the slopes and the breaking of the solitary wave but only focused on the impact, while the solitary experiments of [45,46] show that the ramp slope plays an important role in the breaking of a solitary wave.

In this study, we are interested in investigating which mechanism, whether a solitary wave, dam-break wave, or breaking solitary wave, should be more suitable as a tsunami-like bore. Only with the proper tsunami-like bore can the interaction between the wave and structure be confirmed with confidence.

This study concerns the impact of breaking solitary waves on a horizontal deck. As shown by [3], the breaking has an additional effect on the bore impact on coastal structures. Hence, we studied two breaking waves, namely the solitary breaking wave and dam-break wave. A solitary wave propagates over a submerged ramp and breaks over the shelf, where a horizontal deck is located. In order to compare the breaking solitary wave with the dam-break bore, various slopes from 1:20 to 1:0 (step) were used to find a proper way to break the solitary wave.

The Navier–Stokes equations used to study this problem and the setup of the numerical experiments are introduced in Section 2. The details of the method of breaking are presented in Section 3. Two comparisons with existing laboratory experiments are provided, followed

by the results of the simulations of the breaking solitary wave cases and the dam-break cases. The paper is closed with concluding remarks.

2. The Theory and Numerical Setup

The Navier–Stokes (NS) equations were used in this study, and are discussed in this section, followed by the information of the cases and a grid study for the computations. We adopted a right-handed two-dimensional (2D) Cartesian coordinate system, with x_1 pointing to the right and x_2 pointing vertically opposite to the direction of the gravitational acceleration ($x_2 = 0$ corresponds to the still-water level). Indicial notation and Einstein’s summation convention are used. Subscripts after commas indicate differentiation.

2.1. The Navier–Stokes Equations

For a homogeneous, Newtonian, and incompressible fluid, the flow is governed by the following conservation of mass and momentum equations:

$$u_{i,i} = 0, \quad i = 1, 2 \tag{1}$$

$$u_{j,t} + (u_i u_j)_{,i} = g_j - \frac{1}{\rho} p_{,j} + \nu u_{j,ii}, \quad i, j = 1, 2 \tag{2}$$

where $\vec{u} = u_i \vec{e}_i$ is the velocity vector, \vec{e}_i is the unit normal vector in the i direction, ρ is the density of the fluid, ν is kinematic viscosity, $\vec{g} = (0, -g, 0)$ is the gravitational acceleration, and p is the pressure.

The governing equations are solved for air and water simultaneously. The volume of fluid (VOF) method, originally introduced by [47], is used to determine the free surface between air and water. A scale function is used to represent the volume of fluid in each cell; see [47]. The finite volume approach is used to discretize the equations. The Euler scheme is used for time discretization, and Gauss linear is used for space discretization. The open-source computational fluid dynamics package, OpenFOAM, is used to compute the NS equations. Boundary conditions used in this study are presented in Table 1, where β is the parameter used in the VOF method to present the water component and air component. Details of these boundary conditions can be found in, e.g., [48,49].

Table 1. Boundary conditions used in this study. The boundary conditions definition can be found in, e.g., [48,49].

Boundary	β	p	u
bottom	zeroGradient	zeroGradient	fixedValue (0,0,0)
front and back walls	zeroGradient	zeroGradient	fixedValue (0,0,0)
upwave and downwave atmosphere	inletOutlet	totalPressure	pressureInletOutletVelocity

2.2. Numerical Setup

The results are given in dimensionless form using the density of water, ρ , gravitational acceleration, g , and h as a dimensionally independent set. Therefore, the dimensionless form of time is $t' = t \times \sqrt{g/h}$, the distance is $L' = L/h$, the pressure is $p' = p/(\rho gh)$, and the two-dimensional force is $F' = F/(\rho ghS)$, where $S = T_D b$ for horizontal force F_H , and $S = L_D b$ for vertical force F_V . T_D is the thickness of the deck, and L_D is the length of the deck in the wave propagation direction, as shown in Figure 1. We note that the two-dimensional force is given per unit width into the page, and b is the width of the deck into the page. For simplicity, we drop prime from all variables.

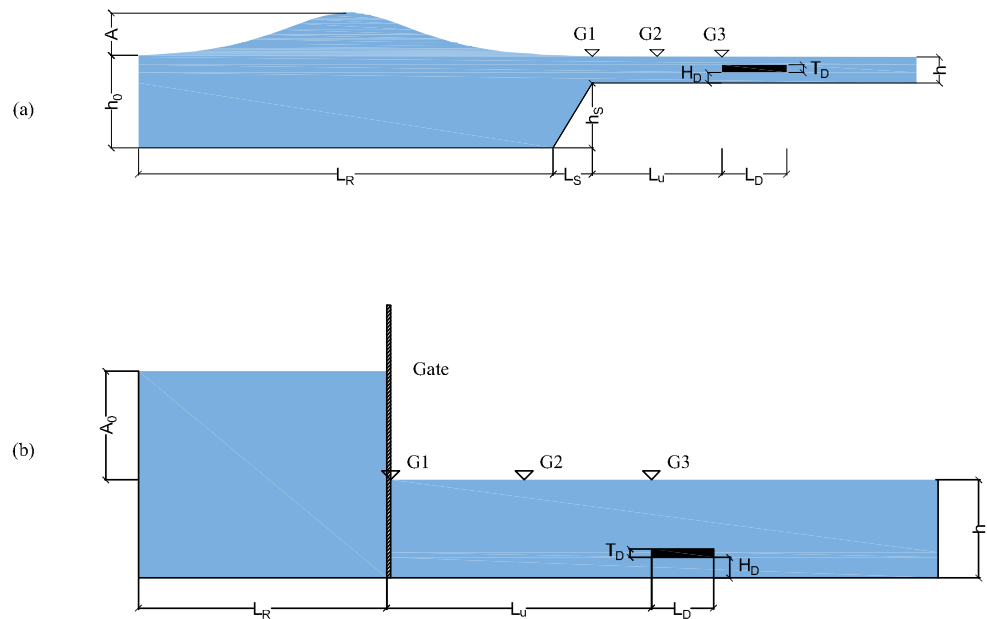


Figure 1. Schematic of the numerical tank of (a) solitary wave propagating over a bottom ramp/step and impacting a horizontal deck and (b) dam-break impact on a horizontal deck case. (Not to scale).

Two Intel Xeon E5-2697A v4 processors (16 cores, 40 M Cache, 3.00 GHz) were used for the NS computations. The maximum Courant number is 0.25, which has been examined by our previous study—see [50]—and the average Courant number is 0.0086. The other settings in OpenFOAM are all kept default; for details, see [48].

A grid convergence study was performed to determine the appropriate grid for the solitary wave breaking computations. For the convergence study, we looked into the solitary wave propagating over a submerged ramp (in the absence of a structure). In the convergence study, the solitary wave amplitude was $A = 1.70$, and the upwave water depth was $h_0 = 4.5$.

Five uniform grids are considered in this part, which is summarized in Table 2. All computations were performed in two dimensions. All cases were computed in OpenFOAM 4.0 extension, and the wave was generated by waves2FOAM; see [51].

Table 2. Grid information of the convergence tests of solitary wave propagating over a submerged ramp.

Grid ID	Δx_1	Δx_2	Number of Cells		Computation
			x_1	x_2	Duration
1	0.169	0.419	335	57,42	8 min
2	0.100	0.251	558	95,70	44 min
3	0.067	0.167	837	142,105	3 h
4	0.033	0.084	1673	284,209	35 h
5	0.017	0.042	3345	568,418	16 days

Comparisons of the surface elevation time series of the five grids at the top of the ramp are shown in Figure 2, where ζ is the free surface elevation. The results of Grids 2, 3, 4, and 5 are in good agreement. Here, Grid 3 was chosen for the solitary wave study.

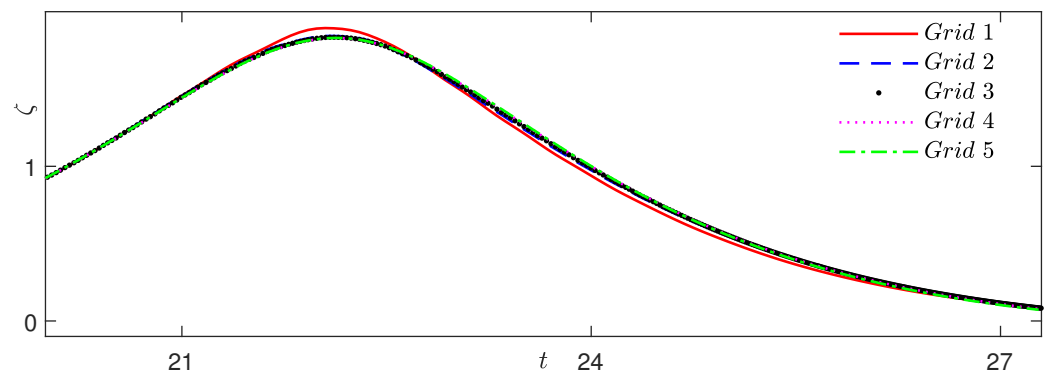


Figure 2. The grid convergence study of solitary-wave-breaking case: comparisons of surface elevation recorded by G1.

3. Bore Generated by Breaking of a Solitary Wave

In this study, we considered the impact of a bore on a deck. The bores are generated by (i) the breaking of a solitary wave and (ii) the breaking of the dam of a reservoir (dam-break).

As the initial shape and form of the solitary wave and the dam-break are different, a reasonable way to compare these two breaking mechanisms is introduced in this section. Figure 1a shows a schematic of the numerical tank where the solitary-wave-breaking bore is studied. The solitary wave breaks when the downwave water depth decreases sufficiently. The schematic of the numerical tank of the dam-break case is shown in Figure 1b.

In this study, h_0 is the upwave water depth, L_u is the distance from the top ramp to the leading edge of the deck, $R = h_s/L_s$ is the slope of the ramp, where $h_s = h_0 - h$ is the vertical height from the bottom of the upwave tank to the bottom of the downwave tank, and L_s is the horizontal length from the trail of the upwave tank to the head of the downwave tank. In all solitary wave cases, the ramp top position is set at $x_1 = 0$.

At the time $t = 0$, the solitary wave propagates from upwave to downwave (left to right), and the solitary wave crest is at $x_1 = -\lambda_e/2$, where λ_e is the effective wavelength of the solitary wave. $\zeta(x_1) \geq 0.001A$ is used as the criteria to determine the upwave and downwave boundary of λ_e , which means the wave starts from the upwave point where $\zeta(x_1) = 0.001A$ and ends at the downwave point where $\zeta(x_1) = 0.001A$. After propagating over the ramp, the solitary wave breaks into a bore with long tail waves. The shape of the initial solitary wave varies with A and h_0 ; see [52]. The generated bore varies according to the slope of the ramp. Appropriate values of A , h_0 , and R are discussed in the following sections.

3.1. Equivalent Solitary Wave

According to Equation (3), where $S_{solitary}$ is the area between the surface elevation of the solitary wave and SWL (still-water level), the shape of the solitary wave is related to two variables, namely A and h_0 . Hence, two conditions are required to find the most appropriate solitary wave to break, and the shape of the generated bore should be as close as possible to the dam-break bore.

$$S_{solitary} = \int_{-\lambda_e/2}^{\lambda_e/2} \zeta(x_1) dx_1 = \frac{A}{\epsilon} \tanh(\epsilon x_1/2) \Big|_{-\lambda_e}^{\lambda_e}. \tag{3}$$

The first condition is that the mass of the initial water reservoir, M_{dam} , and the solitary wave, $M_{solitary}$, should be the same, i.e., $M_{dam} = M_{solitary}$. As the density of water, ρ , and the width of the tank, W (equal to the unit length in two dimensions), is constant in this study, and $M = \rho WS$, $S_{dam} = S_{solitary}$, where S_{dam} is the cross-section area of the reservoir.

The area of the initial dam is $S_{dam} = A_{dam} \times L_R$, where A_{dam} is the initial height of the water reservoir measured from the SWL and L_R is the initial length of the reservoir, as shown in Figure 1b.

The second condition is to set the overlapping area between the water reservoir and solitary wave, S_o , to be at maximum, which means that S_d shown in Figure 3 should be minimum.

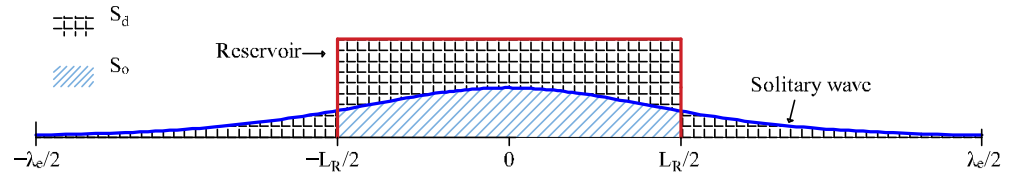


Figure 3. Comparison of the area under an initial reservoir and a solitary wave.

This results in obtaining the closest form between the solitary wave and dam-break. S_o is given as

$$S_o = \int_{-L_R/2}^{L_R/2} \zeta(x_1) dx_1 = \frac{A}{\epsilon} \tanh(\epsilon x_1/2) \Big|_{-L_R}^{L_R}. \tag{4}$$

With these two conditions, the two variables of the initial solitary wave are determined, and the closest agreement between the initial solitary wave and the water reservoir is obtained. This will allow for a fair comparison between bores generated by these two methods.

By considering these two conditions, i.e., using $S_{dam} = S_{solitary}$ and Equation (4), three cases with proper A and h_s , where $h_s = h_0 - h$, were chosen for each solitary-wave-breaking case to compare with three different dam-break cases. These are listed in Table 3.

Table 3. The initial conditions of the dam-break and solitary waves considered in this study.

Case	Dam-Break	Breaking Solitary Wave
1	$A_0 = 2$	$A = 1.70, h_s = 3.5$
2	$A_0 = 5$	$A = 2.72, h_s = 5.5$
3	$A_0 = 8$	$A = 3.40, h_s = 7.0$

3.2. Determination of the Ramp Slope

This section studies the solitary wave bore generation and propagation over the ramp. Twelve cases with different slopes were considered to find a proper ramp slope, listed in Table 4.

Table 4. The slopes considered in this study.

Case	1	2	3	4	5	6	7	8	9	10	11	12
R	1:0	1:1	18:20	17:20	16:20	15:20	10:20	1:3	1:4	1:5	1:15	1:20

The surface elevation is measured at G1 at $x_1 = 0$ (top of the ramp), G2 at $x_1 = 6$, and G3 at $x_1 = 12$. Drastic changes between cases 10 and 8 are found. The surface elevations of cases 10 to 12 have many fluctuations after the bore front, whereas those of cases 1 to 8 are smoother. The results of four (sample) ramp-slope solitary wave cases, Cases 1, 2, 7, 10, with slopes $R = 1:0, 1:1, 1:3, 1:5$, and the corresponding dam-break case are shown in Figure 4.

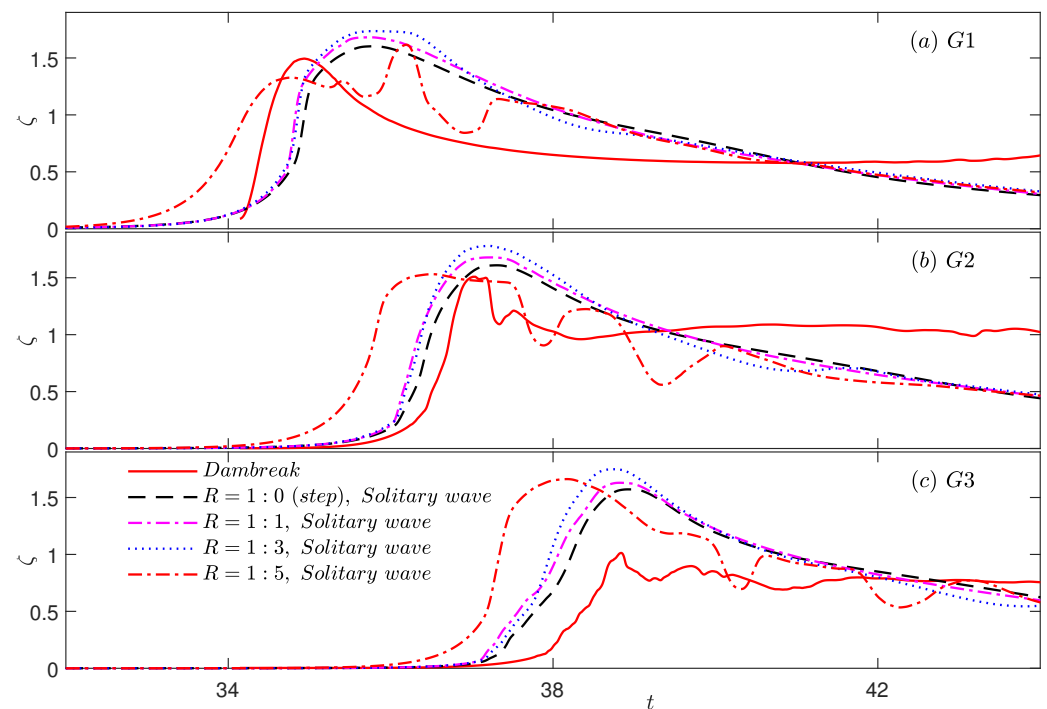


Figure 4. Comparisons of surface elevations recorded by the three gauges, G1, G2, and G3, at $x_1 = 0, 6, 12$, respectively, for an $A = 1.7$ solitary wave propagation over a submerged ramp with various slopes, and the bore generated by equivalent dam-break case with $A_0 = 2$.

Figure 4 shows that the peak elevations of all solitary wave cases are higher than those of the dam-break case. Surface elevations of the case with $R = 1:5$ are the farthest from that of the other three cases. There are two peaks of the surface elevation in this case, whereas only one peak is found in the other solitary wave cases. Surface elevations of cases with $R = 1:3, 1:1, 1:0$ are close to each other. Based on these results, the case with $R = 1:0$ (i.e., step) agrees best with the dam-break case. Hence, $R = 1:0$ was chosen for the rest of the study.

3.3. Determination of the Deck Location

Bores generated by the breaking of a solitary wave or an initial reservoir are unsteady and change shape as they propagate downwave of the ramp. In this section, we discuss an appropriate location for the deck, where the profile of the two bores are close, such that a fair comparison between the solitary wave and reservoir case can be made. To find the position, comparisons were made between surface elevations recorded by gauges at $x_1 = 12$ in the dam-break cases and at $x_1 = 12, 13, 14, \dots, 30$ in the solitary-wave-breaking cases. Three dam-break cases with $A_0 = 2, 5, 8$ were considered in this section, with corresponding three solitary-wave-breaking cases with $A = 1.70, 2.72, 3.40, h_0 = 3.5, 5.5, 7.0$, respectively. There is no deck in this section.

In total, six cases were considered to investigate the appropriate deck location. The solitary wave surface elevations with various L_u, A , and h_0 were studied in these six cases. The results were compared with the dam-break surface elevation at $x_1 = 12$. For all three dam-break cases with $A_0 = 2, 5$, and 8 , the surface elevation of all three solitary wave cases with $x_1 = 12$ is far from that of the respective dam-break cases, and that of the solitary wave cases with $L_u = 21$ is the closest one. The results of the solitary wave case with $A = 1.70$ and $h_0 = 3.5$ and the dam-break case with $A_0 = 2$ are shown in Figure 5 for comparison.

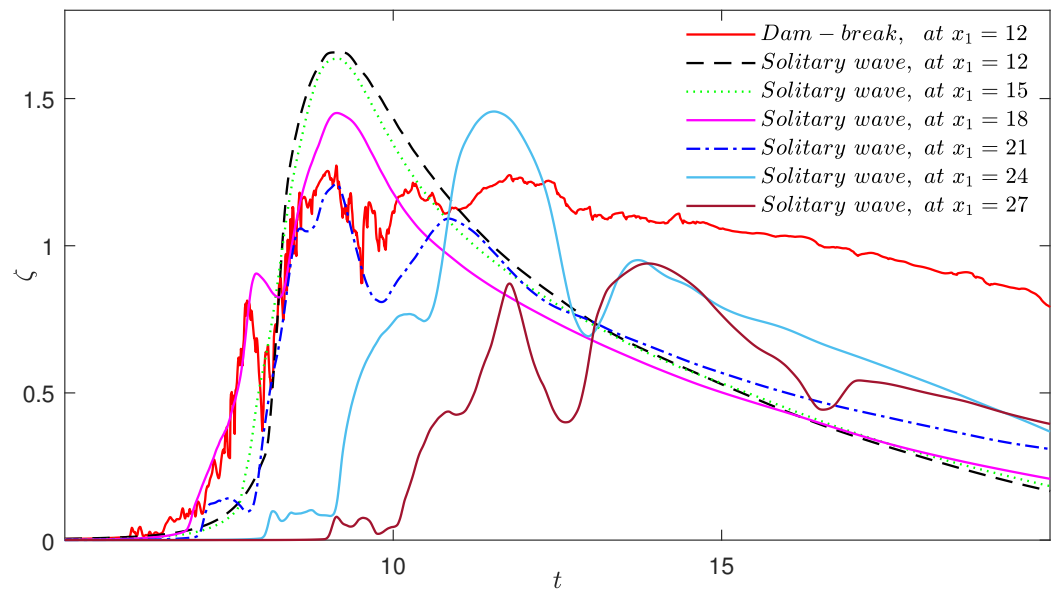


Figure 5. Surface elevation of dam-break (at $x_1 = 12$ downwave from the gate) vs. solitary wave at two different downwave locations, in the absence of the deck, $A_0 = 2$ and $L_R = 12$ in dam-break case, and $A = 1.70$, $h_0 = 3.5$ in solitary wave case.

Figure 5 shows that the solitary-wave surface elevation at $x_1 = 21$ gives the closest agreement with the dam-break surface elevation before $t = 11.5$, whereas the solitary-wave surface elevation at $x_1 = 12$ is higher than dam-break before $t = 11.5$. It is concluded that the solitary wave at $x_1 = 21$ is more suitable for comparison with the dam-break bore.

Snapshots of the solitary wave propagating over a submerged step, (a) without a deck, or with a downwave deck whose leading edge is at (b) $x_1 = 12$, or (c) $x_1 = 21$, are shown in Figure 6. The two dashed lines show the position of the leading edge of the deck at $x_1 = 12$ in Figure 6b and at $x_1 = 21$ in Figure 6c, respectively.

Figure 6a shows the solitary wave profile changes as it propagates over the submerged step at $x_1 = 0$. Beyond $x_1 = 21$, the solitary wave disperses into several small waves. The solitary wave profile changes as it propagates.

In Figure 6b,c, the evolution of the solitary wave profile shows little change due to the presence of the submerged deck before meeting with the deck, which can be proved by the snapshots of the solitary wave taken between t_4 and t_6 in these sub-figures. The wave profiles of Figure 6a,c are closer to each other than that of Figure 6b. The wave profiles of Figure 6a,c show some differences from each other after t_7 when the wave passes over the deck, which means that the deck plays a critical role in the evolution of the solitary wave profile.

Consider the solitary wave shape, the ramp slope, and the deck location. Three groups of solitary-wave-breaking cases are compared against dam-break cases. The information on the groups is listed in Table 5.

Table 5. The initial conditions of the dam-break and solitary waves considered in this study. For the solitary wave, two different locations of the deck, $L_u = 12$ and $L_u = 21$, are considered.

Case	Dam-Break	Breaking Solitary Wave	Deck Level from Bottom
1	$A_0 = 2$	$A = 1.70, h_s = 3.5$	$H_D = 0.4, 0.6, 0.8, 1, 1.5$
2	$A_0 = 5$	$A = 2.72, h_s = 5.5$	
3	$A_0 = 8$	$A = 3.40, h_s = 7.0$	

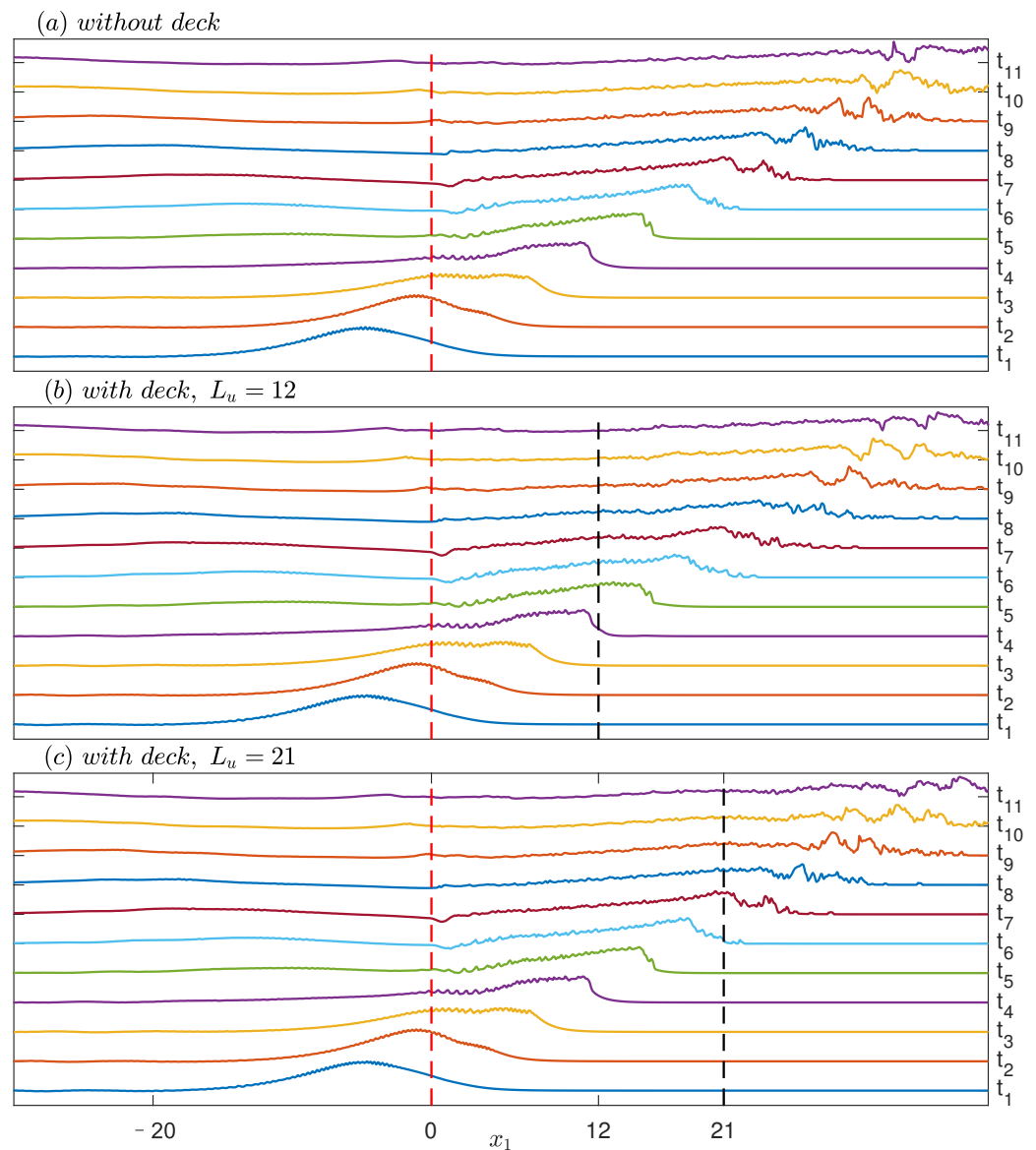


Figure 6. Evolution of a solitary wave propagating over a step (at $x_1 = 0$) eleven times, where $t_1 = 28.77$, $t_{i+1} = t_i + 2$ ($i = 1, 2, 3 \dots 10$). Three different downwave conditions are presented: (a) with no deck downwave; (b) with a deck with $L_u = 12$; (c) with a deck with $L_u = 21$. In these cases, $h_0 = 3.5$, $A = 1.7$, $H_D = 0.4$, and $L_D = 3$ for cases (b,c). The solid (red) line shows the position of the step, and the dashed (black) lines shows the positions of the leading edge of deck for cases (b,c).

4. Comparisons with Experiments

Comparisons of the model’s results with available laboratory experiments are presented here. First, the surface elevations of a solitary wave propagating over a submerged step were considered, followed by the surface elevations and impacts of a solitary wave on a submerged deck.

Seabra-Santos et al. [53] carried out experiments to study the propagation of solitary waves over a downwave step in the long channel of the Institut de Mécanique de Grenoble. The channel is 36 m long, 0.55 m wide, and 1.30 m deep. In the case considered here, $A = 1.825$, $h_0 = 2$, and $R = 1:0$.

The computed and measured wave surface elevation at wave gauges G_1 at $x_1 = 0$ and G_2 at $x_1 = 30$ of [53] were compared. The comparisons of the time series of surface elevation measured at different gauges are shown in Figure 7. Excellent agreement is observed between the model’s results and the laboratory measurements, indicating that the solitary wave propagation over a step is captured correctly in our model.

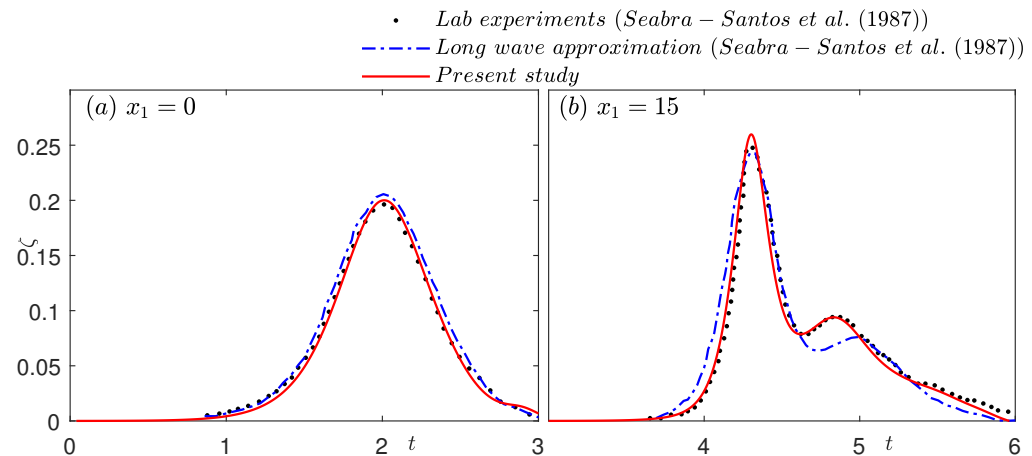


Figure 7. Surface elevation of solitary wave propagating over a step, recorded at two wave gauges showing comparisons between NS equations, long wave equations, and [53]’s lab experiments. In [53]’s laboratory experiments, a solitary wave ($A = 1.825$) propagates over a step at $x_1 = 0$, $h_0 = 2$, and $h = 1$.

Seiffert et al. [20] carried out experiments to study the propagation and impact of a solitary wave on a flat deck. The flume is 9.14 m long, 0.152 m wide, and 0.39 m high. A horizontal deck of width $W = 0.149$ m (where the width is defined in the direction into the page), length $L_D = 0.305$ m (where the length is defined in the direction of wave propagation), thickness $T_D = 0.0127$ m, and deck height $H_D = 0.0561$ m was placed downwave. Three wave gauges, G_1 (0.61 m upwave of the leading edge of the deck), G_2 (0.915 m downwave the leading edge of the deck), and G_3 (2.135 m downwave the leading edge of the deck), were used to measure the wave elevations. The horizontal force on the deck was measured by three load cells, whereas the vertical force was measured by one cell. The tank floor was flat in this case.

The computed and measured surface elevations and forces of [20] were compared with the result of this study. The results are shown in Figure 8.

Figure 8a–c show the surface elevations of the solitary wave propagating over the submerged deck, and the results of NS agree well with the experimental data of [20]. Overall, an excellent agreement is observed between the results.

The same analysis was performed on the vertical force and horizontal force results shown in Figure 8d,e, and good agreement is observed.

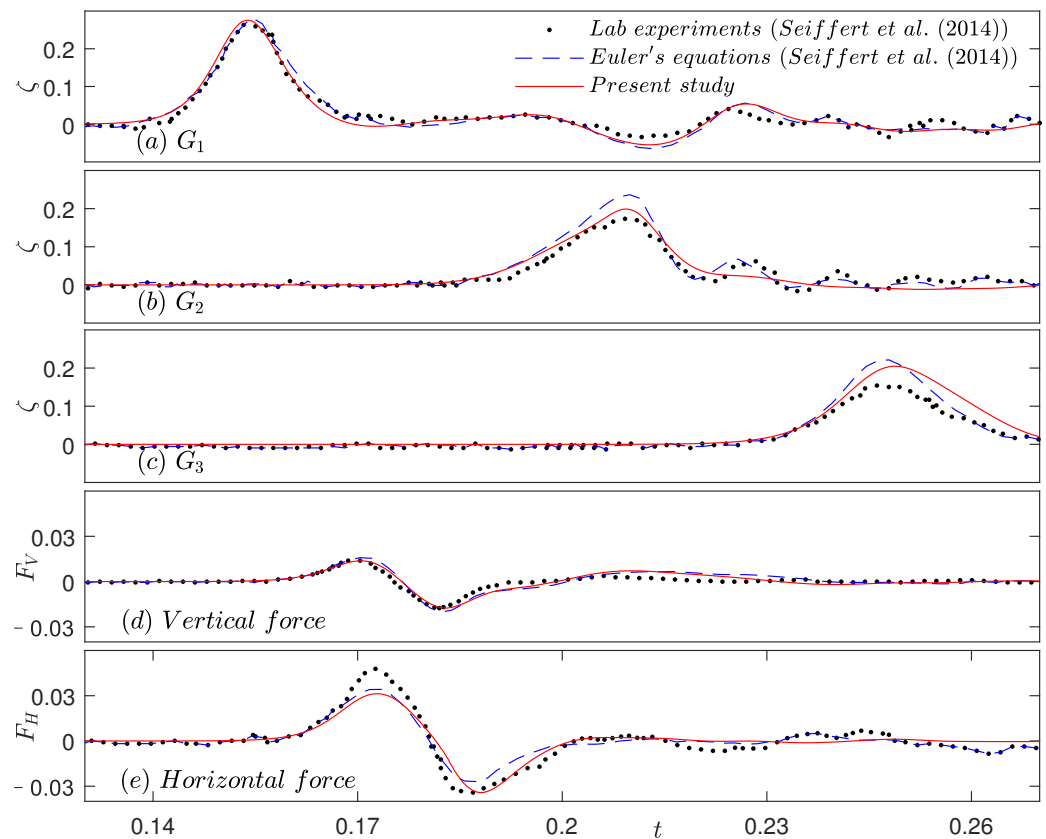


Figure 8. Solitary wave propagating over a submerged deck, (a–c) surface elevation recorded at gauges G1, G2, and G3, respectively, (d) vertical force, and (e) horizontal force. Results of the present study are compared with laboratory experiments and computations of [20], $A = 0.3$.

5. Comparisons between Dam-Break and Breaking Solitary Wave

This section presents the results of bore impact on a horizontal deck for a combination of two bore generation methods and five deck elevations from the seafloor. Solitary waves with three initial amplitudes were considered, and the results were compared with the equivalent dam-break bore. These include I: $A = 1.70$, II: $A = 2.72$, III: $A = 3.40$.

As discussed in the previous section, two locations of the deck were considered, namely $L_u = 12$ and $L_u = 21$, for breaking solitary wave cases. Five vertical positions of the deck were considered, including the submerged positions ($H_D = 0.4, 0.6,$ and 0.8), when the deck is located at the free surface, $H_D = 1$, and when the deck is above the free surface, $H_D = 1.5$. The solitary wave-generated bore impact results were compared with those of the dam-break bore.

Hence, fifteen (3×5) cases were considered in this study, as shown in Table 5. They are solitary wave cases with the leading edge of the deck located at (i) $x_1 = 12$ and (ii) $x_1 = 21$, and (iii) dam-break cases with the leading edge of the deck at $x_1 = 12$. Five different deck elevations were considered for each of the three cases.

5.1. I: $A = 1.70$

The time series of solitary wave horizontal and vertical forces on the deck is shown in Figures 9 and 10, along with the dam-break horizontal and vertical forces for $A = 1.70$, respectively. The peak values of the forces are listed in Table 6.

Table 6. The peak value of the horizontal and vertical force of solitary wave and dam-break on the deck, $A = 1.70$.

H_D	Horizontal Force			Vertical Force		
	Solitary Wave		Dam-Break	Solitary Wave		Dam-Break
	$L_u = 12$	$L_u = 21$		$L_u = 12$	$L_u = 21$	
0.4	2.063	1.326	0.828	2.740	1.755	1.376
0.6	1.687	1.098	0.853	3.258	2.151	2.321
0.8	2.046	1.305	0.794	3.303	3.208	2.128
1	1.785	1.676	1.032	4.127	4.041	2.835
1.5	0.116	0.015	1.091	0.241	0.042	2.408

As expected for both horizontal and vertical forces, the maximum value of the solitary-wave bore is larger when the deck is closer to the step. The maximum value due to the solitary wave (regardless of the deck’s location) is larger than that of the dam-break for all submerged cases, where $H_D \leq 1$. The difference between the solitary waves becomes smaller when the deck is closer to the free surface. In the elevated case, where $H_D = 1.5$, the value force of the solitary-wave bore is significantly smaller than that of the dam-break bore.

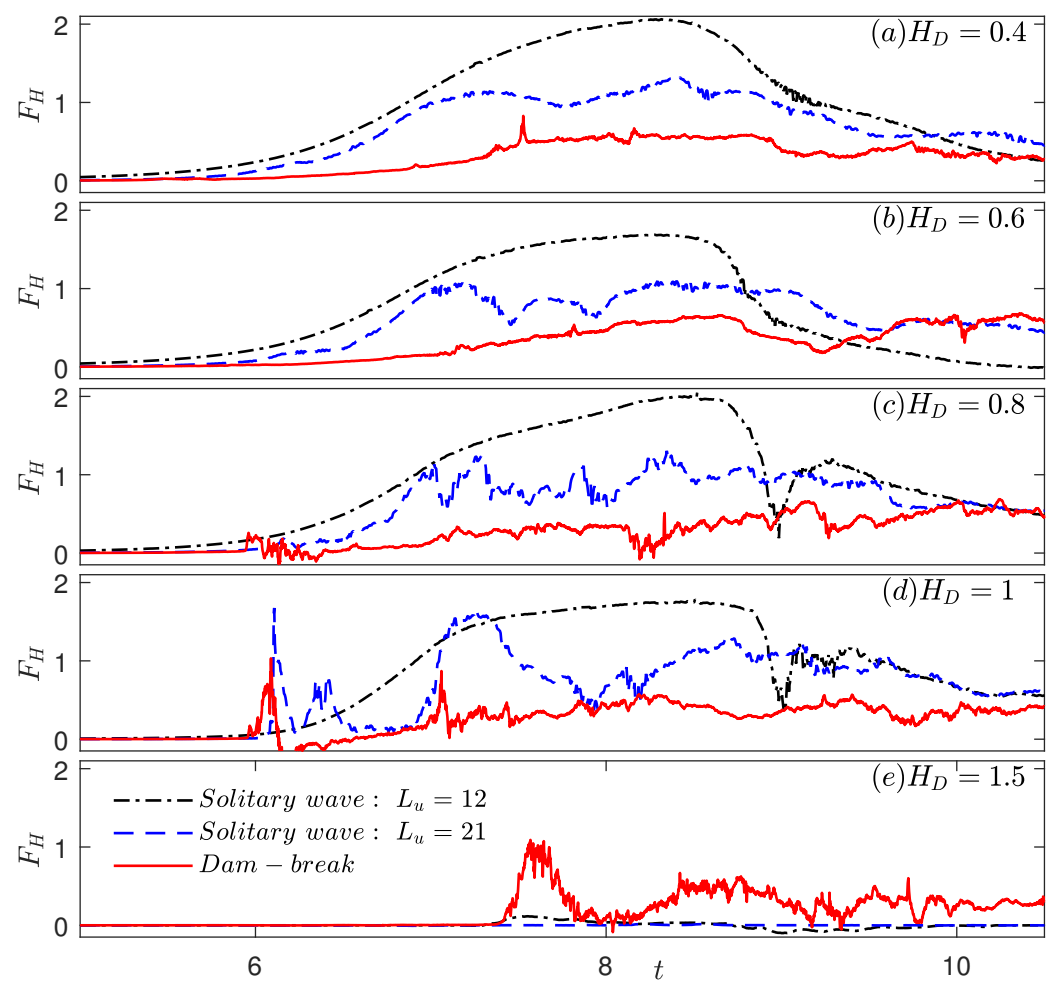


Figure 9. The horizontal force of solitary wave and dam-break on the deck, $A = 1.70$.

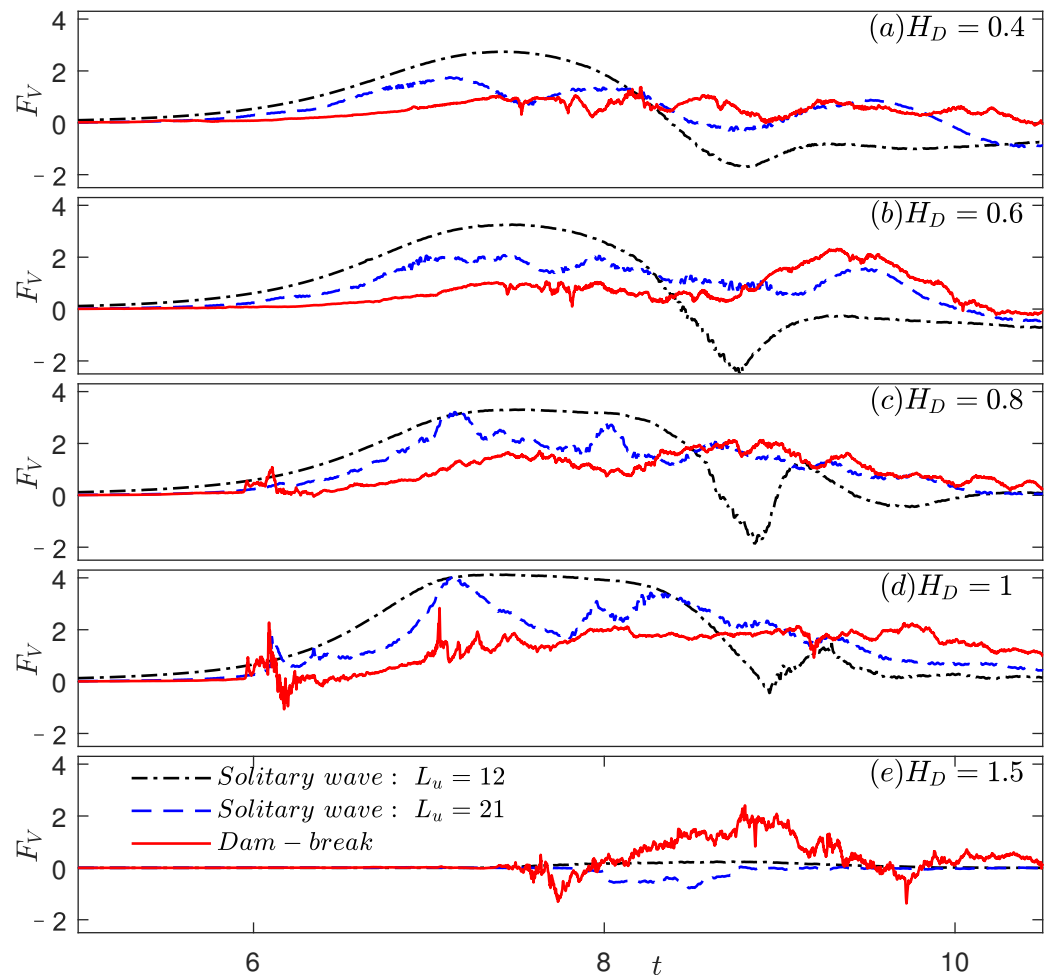


Figure 10. The vertical force of solitary wave and dam-break on the deck, $A = 1.70$.

The previous work of [54], which investigated the dam break bore impact on a bridge superstructure, found significant impulsive uplift forces followed by downward forces. The impulsive uplift component is non-existent or has a minor role in Figure 9. However, it had a governing role in [54].

The bore’s uplift force on the deck is tightly related to the bore shape. We can compare the bore shape of these two studies between Figure 5 in this study and Figure 2 in [54].

In Figure 5 in this study, the bore’s front foot arrives at the deck at $t = 2$, and the peak arrives at $t = 8$, where the duration is 6. In Figure 2 in [54], the bore’s front foot arrives at the deck at $t = 1.35$, and the peak at $t = 14.5$, where the duration is 1. The duration in this study is longer than that in [54], which means that the bore’s front in [54] is much steeper than that in this study. Hence, it is easy to find the impulsive uplift component.

Moreover, in this study, the ratio between the reservoir and downstream water depth (A/h) and the vertical position of the deck (H_D) are variables. The vertical force of cases with $H_D = 0.4, 0.6, 0.8,$ and 1 show that no or small impulsive uplift component is reasonable, as the deck’s top is under or on the free surface. The ratio between the reservoir and downstream water depth (A/h) of cases in this study is $1.07, 2.72,$ and 3.40 , which is smaller than the $A/h = 6.2$ of the case shown in Figure 2 in the study in [54].

5.2. II: $A = 2.72$

The time series of solitary wave horizontal and vertical forces on the deck is shown in Figures 11 and 12, along with the dam-break horizontal and vertical forces for $A = 2.72$, respectively. The peak values of the forces are listed in Table 7.

The differences between solitary waves and dam-break waves are smaller than that for $A = 1.70$, especially for vertical force in Figure 12. In the elevated case, the peak value of the horizontal force of solitary waves is larger than the dam-break wave when the deck is further away from the step.

5.3. III: $A = 3.40$

The time series of solitary wave horizontal and vertical forces on the deck is shown in Figures 13 and 14, along with the dam-break horizontal and vertical forces for $A = 3.40$, respectively. The peak values of the forces are listed in Table 8.

Table 7. The peak value of the horizontal and vertical force of solitary wave and dam-break on the deck, $A = 2.72$.

H_D	Horizontal Force			Vertical Force		
	Solitary Wave		Dam-Break	Solitary Wave		Dam-Break
	$L_u = 12$	$L_u = 21$		$L_u = 12$	$L_u = 21$	
0.4	3.421	2.627	1.794	3.908	5.417	5.268
0.6	2.833	2.164	1.391	4.675	8.183	6.203
0.8	3.424	2.231	2.015	4.874	7.889	5.620
1	3.155	4.110	2.604	6.086	8.863	6.166
1.5	0.711	11.066	3.042	0.557	1.904	7.747

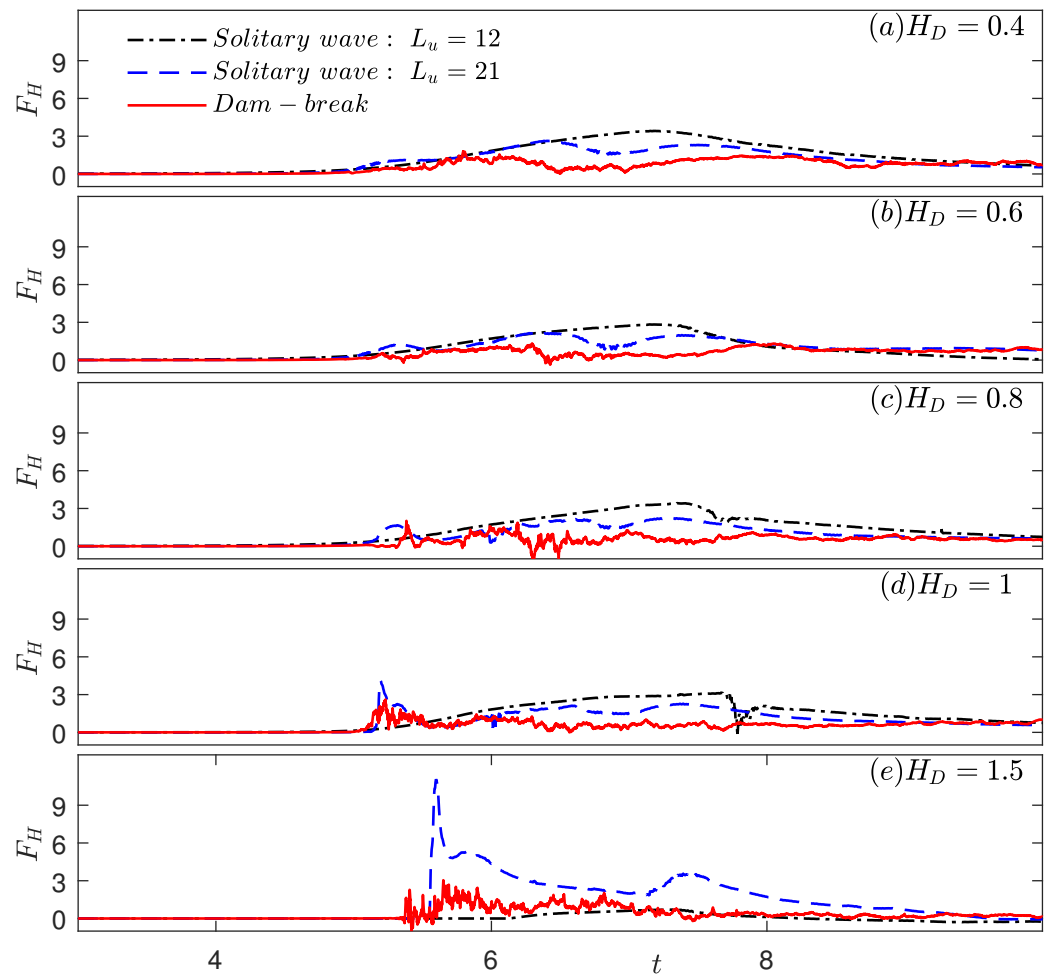


Figure 11. The horizontal force of solitary wave and dam-break on the deck, $A = 2.72$.

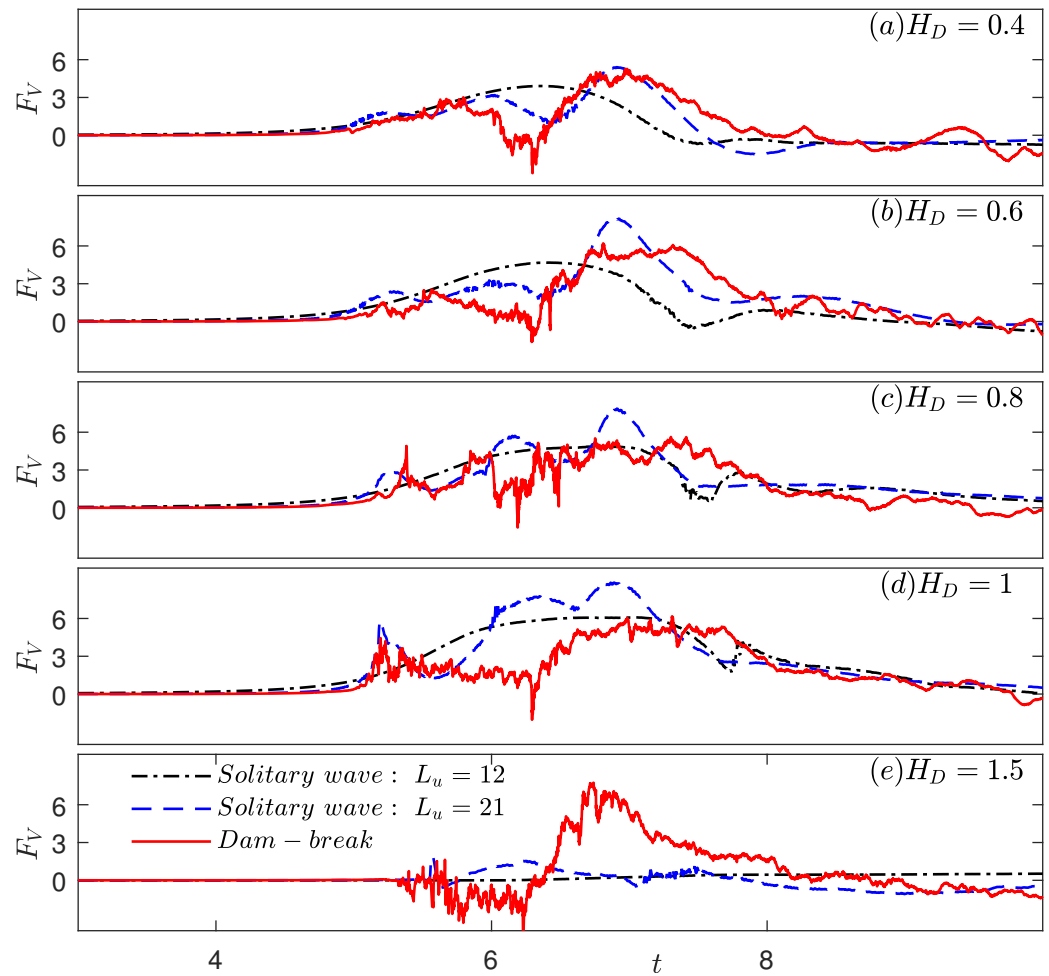


Figure 12. The vertical force of solitary wave and dam-break on the deck, $A = 2.72$.

Table 8. The peak value of the horizontal and vertical force of solitary wave and dam-break on the deck, $A = 3.40$.

H_D	Horizontal Force			Vertical Force		
	Solitary Wave		Dam-Break	Solitary Wave		Dam-Break
	$L_u = 12$	$L_u = 21$		$L_u = 12$	$L_u = 21$	
0.4	4.014	3.695	4.682	4.213	7.556	10.941
0.6	3.354	2.849	6.672	5.088	10.609	12.762
0.8	4.109	3.584	4.188	5.581	10.217	14.432
1	4.002	3.273	4.317	7.306	11.876	17.284
1.5	0.989	12.799	4.998	0.476	4.246	18.140

The horizontal force of the solitary-wave bore is in closer agreement with the dam-break force in the submerged case, $H_D \leq 1.0$. In the unsubmerged case, the peak value of the horizontal force of solitary waves is larger than the dam-break wave when the deck is further away from the step, also found in II: $A = 2.72$.

The vertical force of the solitary-wave bore is smaller than the dam-break force, which is different from that in I: $A = 1.70$ and II: $A = 2.72$.

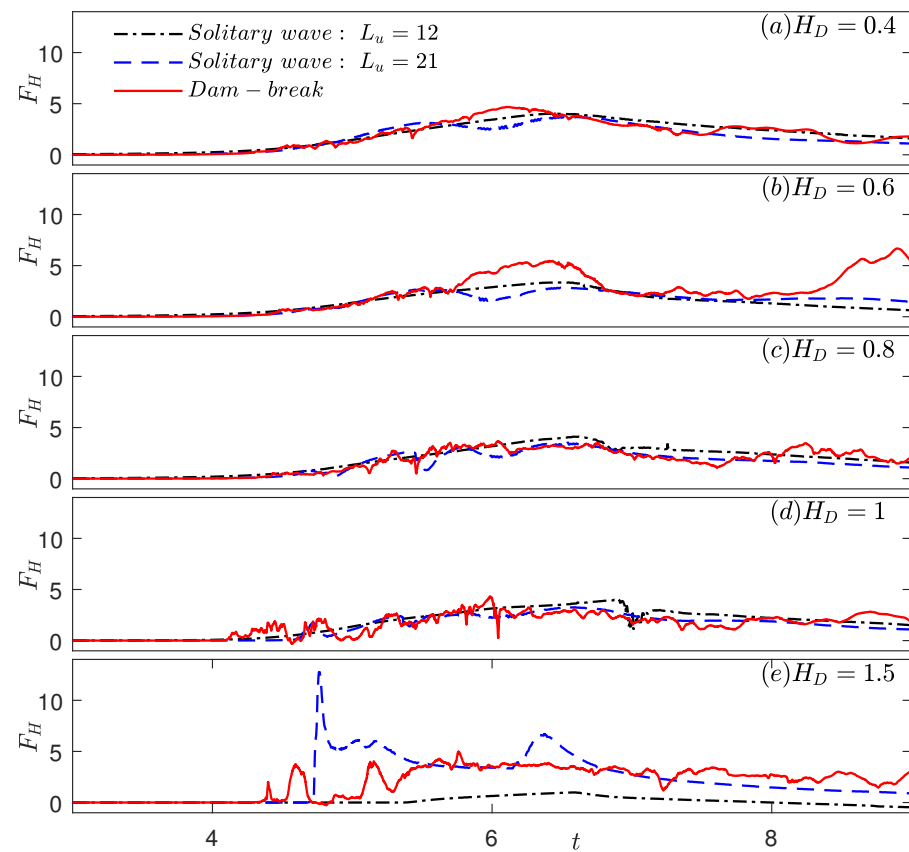


Figure 13. The horizontal force of solitary wave and dam-break on the deck, $A = 3.40$.

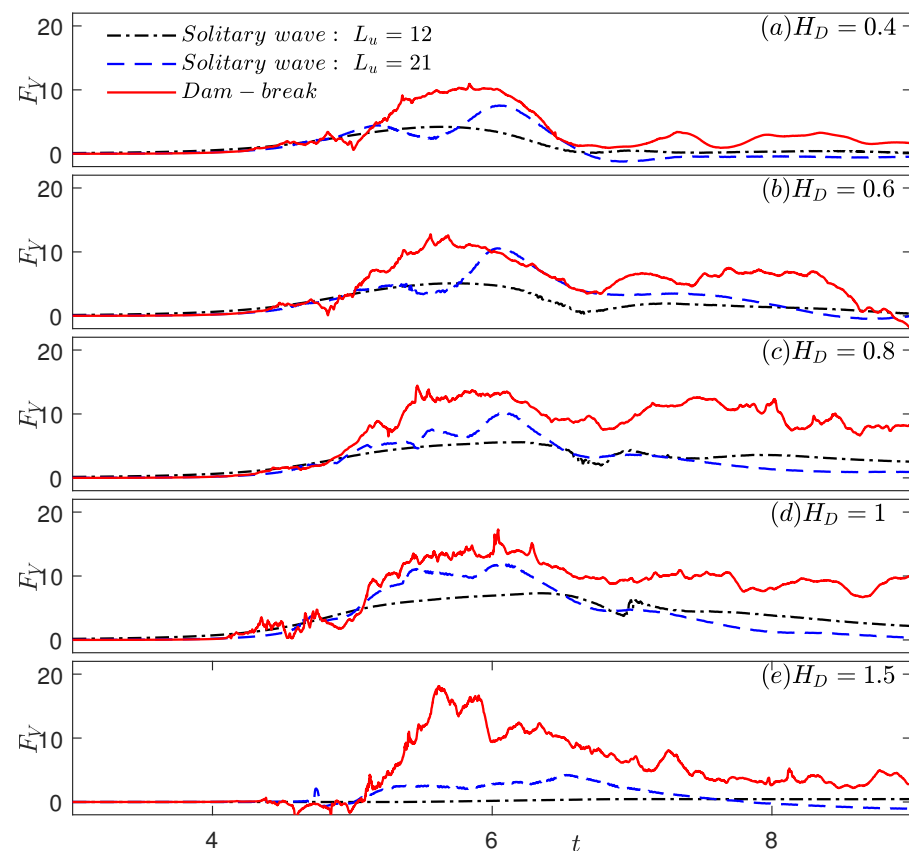


Figure 14. The vertical force force of solitary wave and dam-break on the deck, $A = 3.40$.

6. Concluding Remarks

The impact of bores generated by breaking solitary waves over a submerged step was studied using computational fluid dynamics. The proper method for breaking a solitary wave is discussed. The tsunami-like bores generated by different methods were compared. In order to study the effect of the downwave slope on breaking solitary waves, a wide range of seafloor slopes, from 1:20 to 1:0 (step), was used. In the step case, the shape of the generated bore is closer to that of the dam-break bore. The bore is unsteady. It changes its form as it propagates. The propagation distance is important in the bore shape and impact on the downwave structures. An appropriate location for the deck is defined by considering a range of locations downwave of the step. The results show that a breaking solitary wave takes a longer distance to form the same bore shape as the dam-break bore. A comparable solitary wave to dam-break was studied by determining appropriate values for the wave amplitude and water depth. Given that the bore generated by the solitary wave is unsteady, the discussion is provided on the appropriate deck location to allow for a fair comparison.

For submerged structures, the force of the solitary-wave bore is larger than the dam-break bore. For structures above the free surface, the horizontal force of the solitary-wave case is smaller, whereas the vertical force of the solitary-wave bore is larger. By increasing the initial amplitude, an increase in impacts on the deck for solitary-wave bores and dam-break bores is expected. A more significant increase is observed for the impacts of solitary-wave cases when the deck is further away from the step and dam-break cases. The maximum impact of the solitary-wave bore is larger when the deck is closer to the step. The impact of the solitary wave is smoother when the deck is closer to the step, which shows that the breaking solitary wave is less turbulent at that position. In all submerged cases, where $H_D \leq 1$, the maximum value due to the solitary wave (regardless of the deck's location) is larger than that of the dam-break. The difference becomes smaller when the deck is closer to the free surface. The force of the solitary-wave bore is in closer agreement with the dam-break force when the deck is further from the step. The results are complicated in the unsubmerged cases, where $H_D = 1.5$, as the free surface varies for different initial amplitudes. For a small initial amplitude, $A = 1.70$, the value force of the solitary-wave bore is significantly smaller than that of the dam-break bore. For a large initial amplitude, $A = 2.72, 3.40$, the maximum horizontal force due to the solitary wave with a farther deck is larger than that of the dam-break case. In comparison, the maximum vertical force due to the solitary wave with a farther deck is smaller than that of the dam-break case.

Hence, a breaking solitary wave is suggested to be used as a tsunami-like bore in studying the tsunami impact on structures, as the peak value is larger than the dam-break wave when the amplitude is small. For large-amplitude tsunami conditions, dam-break appears to provide more conservative loading on the deck.

There are many ways to find equivalent solitary waves and dam-break bores. We considered the initial velocity, height, and even equivalent length. There is much work that can be carried out and discussed on this topic. Velocity is a good option, but the velocity of the dam-break bore is not constant during propagation. The velocity of a solitary wave after breaking is complex to determine. Velocity in this study was one of the most complex variables that we dealt with. It would be more complex if velocity were picked. This study tries to distinguish between the breaking solitary wave and the dam-breaking bore. Hence, we fixed the volume of the water, which was easier to be fixed in this study, and discuss the complicated variables such as velocity and force. This study will be carried on. Our further study will discuss all parameters, such as velocity and height.

Many works could be carried out in the future. More details about the difference between the dam-break bore and breaking solitary wave could be discussed by comparing the particle velocity around the horizontal deck. The overturning moment on the deck also plays an important role in the bridge's destruction; see [22,55]. Simplified force equations could be derived for the impact of a bore generated by dam-break and a breaking solitary wave, such as [56], which related the length of the deck with the solitary-wave-induced

uplift forces. The dynamic fluid–structure interaction of bridges and the effect of structural flexibility could be considered, such as [57,58], which proved that this kind of structure can reduce the tsunami forces significantly. The various length scales and time scales involved in the bore’s evolution also need to be studied in the future.

Author Contributions: Conceptualization, M.H.; Methodology, M.H.; Software, J.L. and M.H.; Validation, J.L. and M.H.; Formal analysis, J.L.; Investigation, J.L. and M.H.; Resources, M.H.; Writing—original draft, J.L.; Writing—review and editing, M.H.; Visualization, J.L.; Supervision, M.H.; Project administration, M.H. All authors have read and agreed to the published version of the manuscript.

Funding: This research received no external funding.

Data Availability Statement: The data that support the findings of this study are available within the article.

Conflicts of Interest: The authors declare no conflict of interest.

References

- Cox, D. The inappropriate tsunami icon. *Sci. Tsunami Hazards* **2001**, *9*, 87–92.
- Matsuyama, M.; Ikeno, M.; Sakakiyama, T.; Takeda, T. A study of tsunami wave fission in an undistorted experiment. In *Tsunami and Its Hazards in the Indian and Pacific Oceans*; Springer: Berlin/Heidelberg, Germany, 2007; pp. 617–631.
- Madsen, P.; Fuhrman, D.; Schäffer, H. On the solitary wave paradigm for tsunamis. *J. Geophys. Res.* **2008**, *113*, 1–22. [[CrossRef](#)]
- Felton, E.A.; Crook, K.A. Evaluating the impacts of huge waves on rocky shorelines: An essay review of the book ‘Tsunami—The Underrated Hazard’. *Mar. Geol.* **2003**, *197*, 1–12. [[CrossRef](#)]
- Cluff, L.S. Effects of the 2004 Sumatra-Andaman earthquake and Indian ocean tsunami in Aceh province. *Bridge* **2007**, *37*, 12–16.
- JSCE (Japan Society of Civil Engineers). *Valuation of Tsunami Force Acting on Bridge Structures*; Technical Report; JSCE (Japan Society of Civil Engineers): Tokyo, Japan, 1994.
- Maruyama, Y.; Kitamura, K.; Yamazaki, F. Estimation of Tsunami-Inundated Areas in Asahi City, Chiba Prefecture, after the 2011 off the Pacific Coast of Tohoku Earthquake based on Satellite Images and Numerical Simulation. *Earth. Spec.* **2013**, *29*, 201–217. [[CrossRef](#)]
- Weggel, J.R. Maximum breaker height for design. In *Coastal Engineering 1972*; American Society of Civil Engineers: Washington, DC, USA, 1973; pp. 419–432.
- Grimshaw, R. The solitary wave in water of variable depth. *J. Fluid Mech.* **1970**, *42*, 639–656. [[CrossRef](#)]
- Benilov, E.S.; Flanagan, J.D.; Howlin, C.P. Evolution of packets of surface gravity waves over smooth topography. *J. Fluid Mech.* **2005**, *533*, 171–181. [[CrossRef](#)]
- Grimshaw, R.; Annenkov, S. Water Wave Packets Over Variable Depth. *Stud. Appl. Math.* **2011**, *126*, 409–428. [[CrossRef](#)]
- Rajan, G.K.; Bayram, S.; Henderson, D.M. Periodic envelopes of waves over non-uniform depth. *Phys. Fluids* **2016**, *28*, 042106. [[CrossRef](#)]
- Djordjević, V.; Redekopp, L. On the development of packets of surface gravity waves moving over an uneven bottom. *J. Appl. Math. Phys.* **1978**, *29*, 950–962. [[CrossRef](#)]
- Nik Ismail, N.N.A.; Alias, A.; Harun, F.N. The Propagation of Nonlinear Internal Waves under the Influence of Variable Topography and Earth’s Rotation in a Two-Layer Fluid. *Fluids* **2020**, *5*, 140. [[CrossRef](#)]
- Korteweg, D.J.; de Vries, G. On the change of form of long waves advancing in a rectangular canal, and on a new type of long stationary waves. *Philos. Mag.* **1895**, *39*, 422–433. [[CrossRef](#)]
- Wang, A.; Zong, Z.; Zou, L.; Pei, Y.; Hu, Y. Experimental observation of O-solitary waves in shallow water. *Phys. Fluids* **2021**, *33*, 127114. [[CrossRef](#)]
- Quezada de Luna, M.; Ketcheson, D.I. Solitary water waves created by variations in bathymetry. *J. Fluid Mech.* **2021**, *917*, A45. [[CrossRef](#)]
- Bradner, C.; Schumacher, T.; Cox, D.; Higgins, C. Experimental setup for a large-scale bridge superstructure model subjected to waves. *J. Waterw. Port Coast. Ocean. Eng.* **2011**, *137*, 3–11. [[CrossRef](#)]
- Hoshikuma, J.; Zhang, G.; Nakao, H.; Sumimura, T. Tsunami-induced effects on girder bridges. In Proceedings of the International Symposium for Bridge Earthquake Engineering in Honor of Retirement of Professor Kazuhiko Kawashima, Tokyo, Japan, 11–13 September 2013; p. 102.
- Seiffert, B.; Hayatdavoodi, M.; Ertekin, R.C. Experiments and computations of solitary-wave forces on a coastal-bridge deck. Part I: Flat plate. *Coast. Eng.* **2014**, *88*, 194–209. [[CrossRef](#)]
- Istrati, D.; Buckle, I.; Lomonaco, P.; Yim, S. Deciphering the Tsunami Wave Impact and Associated Connection Forces in Open-Girder Coastal Bridges. *J. Mar. Sci. Eng.* **2018**, *6*, 148. [[CrossRef](#)]
- Xiang, T.; Istrati, D.; Yim, S.C.; Buckle, I.G.; Lomonaco, P. Tsunami loads on a representative coastal bridge deck: Experimental study and validation of design equations. *J. Waterw. Port Coast. Ocean. Eng.* **2020**, *146*, 04020022. [[CrossRef](#)]

23. Istrati, D.; Buckle, I.G. *Tsunami Loads on Straight and Skewed Bridges—Part 1: Experimental Investigation and Design Recommendations (No. FHWA-OR-RD-21-12)*; Technical Report; Oregon. Dept. of Transportation. Research Section: Salem, OR, USA, 2021.
24. Siew, P.; Hurley, D. Long surface waves incident on a submerged horizontal plate. *J. Fluid Mech.* **1977**, *83*, 141–151. [[CrossRef](#)]
25. Hayatdavoodi, M.; Seiffert, B.; Ertekin, R.C. Experiments and calculations of cnoidal wave loads on a flat plate in shallow-water. *J. Ocean. Eng. Mar. Energy* **2015**, *1*, 77–99. [[CrossRef](#)]
26. Azadbakht, M. *Tsunami and Hurricane Wave Loads on Bridge Superstructures*. Ph.D. Thesis, Oregon State University, Corvallis, OR, USA, 2014.
27. Istrati, D.; Buckle, I.G. *Tsunami Loads on Straight and Skewed Bridges—Part 2: Numerical Investigation and Design Recommendations (No. FHWA-OR-RD-21-13)*; Technical Report; Oregon. Dept. of Transportation. Research Section: Salem, OR, USA, 2021.
28. Hayatdavoodi, M.; Ertekin, R.C. Wave Forces on a Submerged Horizontal Plate. Part I: Theory and Modelling. *J. Fluids Struct.* **2015**, *54*, 566–579. [[CrossRef](#)]
29. Hayatdavoodi, M.; Liu, J.; Cengiz Ertekin, R. Bore Impact on Decks of Coastal Structures. *J. Waterw. Port Coast. Ocean. Eng.* **2022**, *148*, 04021051. [[CrossRef](#)]
30. Sarfaraz, M.; Pak, A. SPH numerical simulation of tsunami wave forces impinged on bridge superstructures. *Coast. Eng.* **2017**, *121*, 145–157. [[CrossRef](#)]
31. Hasanpour, A.; Istrati, D.; Buckle, I.G. Multi-Physics Modeling of Tsunami Debris Impact on Bridge Decks. In Proceedings of the 3rd International Conference on Natural Hazards and Infrastructure, Athens, Greece, 5–7 July 2022; pp. 1–14.
32. Segur, H. The Korteweg–de Vries equation and water waves. Part 1. Solution of the equation. *J. Fluid Mech.* **1973**, *59*, 721–736. [[CrossRef](#)]
33. Hammack, J.L.; Segur, H. Modelling criteria for long water waves. *J. Fluid Mech.* **1978**, *84*, 359–373. [[CrossRef](#)]
34. Goring, D.G. *Tsunamis—The Propagation of Long Waves onto a Shelf*. Ph.D. Thesis, California Institute of Technology, Pasadena, CA, USA, 1979.
35. Hayashi, H.; Aoki, K.; Shijo, R.; Suzuki, T. Study on tsunami wave force acting on a bridge superstructure. In Proceedings of the 29th US-Japan Bridge Engineering Workshop, Tsukuba, Japan, 11–13 November 2013; pp. 11–13.
36. Chan, I.C.; Liu, P.L.F. On the runup of long waves on a plane beach. *J. Geophys. Res. Ocean.* **2012**, *117*, C08006. [[CrossRef](#)]
37. Hirata, K.; Satake, K.; Tanioka, Y.; Kuragano, T.; Hasegawa, Y.; Hayashi, Y.; Hamada, N. The 2004 Indian Ocean tsunami: Tsunami source model from satellite altimetry. *Earth Planets Space* **2006**, *58*, 195–201. [[CrossRef](#)]
38. Arnason, H.; Petroff, C.; Yeh, H. Tsunami bore impingement onto a vertical column. *J. Disaster Res.* **2009**, *4*, 391–403. [[CrossRef](#)]
39. Robertson, I.N.; Carden, L.P.; Chock, G.Y. Case Study of Tsunami Bore Impact on RC Wall. In Proceedings of the ASME 2013 32nd International Conference on Ocean, Offshore and Arctic Engineering, Nantes, France. American Society of Mechanical Engineers, Nantes, France, 9–14 June 2013; pp. 77–85.
40. Mazinani, I.; Ismail, Z.B.; Shamsirband, S.; Hashim, A.M.; Mansourvar, M.; Zalnezhad, E. Estimation of Tsunami bore forces on a coastal bridge using an extreme learning machine. *Entropy* **2016**, *18*, 167. [[CrossRef](#)]
41. Fathi-Moghadam, M.; Davoudi, L.; Motamedi-Nezhad, A. Modeling of solitary breaking wave force absorption by coastal trees. *Ocean Eng.* **2018**, *169*, 87–98. [[CrossRef](#)]
42. Husrin, S.; Strusińska, A.; Oumeraci, H. Experimental study on tsunami attenuation by mangrove forest. *Earth Planets Space* **2012**, *64*, 973–989. [[CrossRef](#)]
43. Istrati, D. *Large-Scale Experiments of Tsunami Inundation of Bridges including Fluid-Structure-Interaction*. Ph.D. Thesis, University of Nevada, Reno, NV, USA, 2017.
44. Yang, W.; Li, S.; Liu, J.; Wu, W.; Li, H.; Wang, N. Numerical study on breaking solitary wave force on box-girder bridge. *Adv. Bridge Eng.* **2021**, *2*, 28. [[CrossRef](#)]
45. Zelt, J. The run-up of nonbreaking and breaking solitary waves. *Coast. Eng.* **1991**, *15*, 205–246. [[CrossRef](#)]
46. Maiti, S.; Sen, D. Computation of solitary waves during propagation and runup on a slope. *Ocean Eng.* **1999**, *26*, 1063–1083. [[CrossRef](#)]
47. Hirt, C.W.; Nichols, B.D. Volume of fluid (VOF) method for the dynamics of free boundaries. *J. Comput. Phys.* **1981**, *39*, 201–225. [[CrossRef](#)]
48. Greenshields, C.J. *OpenFOAM User Guide*; OpenFOAM Foundation Ltd.: Emilia-Romagna, Italy, 2018; Volume 3.
49. Higuera, P.; Lara, J.L.; Losada, I.J. Realistic wave generation and active wave absorption for Navier–Stokes models: Application to OpenFOAM®. *Coast. Eng.* **2013**, *71*, 102–118. [[CrossRef](#)]
50. Liu, J.; Hayatdavoodi, M.; Ertekin, R.C. On Bore Dynamics and Pressure: RANS, Green-Naghdi, and Saint-Venant Equations. *J. Offshore Mech. Arct. Eng.* **2020**, *142*, 021902. [[CrossRef](#)]
51. Jacobsen, N.G.; Fuhrman, D.R.; Fredsøe, J. A Wave Generation Toolbox for the Open-Source CFD Library: OpenFoam®. *Int. J. Numer. Methods Fluids* **2012**, *70*, 1073–1088. [[CrossRef](#)]
52. Ertekin, R.C.; Hayatdavoodi, M.; Kim, J.W. On some solitary and cnoidal wave diffraction solutions of the Green-Naghdi equations. *Appl. Ocean Res.* **2014**, *47*, 125–137. [[CrossRef](#)]
53. Seabra-Santos, F.J.; Renouard, D.P.; Temperville, A.M. Numerical and experimental study of the transformation of a solitary wave over a shelf or isolated obstacle. *J. Fluid Mech.* **1987**, *176*, 117–134. [[CrossRef](#)]
54. Istrati, D.; Hasanpour, A. Numerical Investigation of Dam Break-Induced Extreme Flooding of Bridge Superstructures. In Proceedings of the 3rd International Conference on Natural Hazards and Infrastructure, Athens, Greece, 5–7 July 2022; pp. 1–15.

55. Bricker, J.D.; Kawashima, K.; Nakayama, A. CFD analysis of bridge deck failure due to tsunami. In Proceedings of the International Symposium on Engineering Lessons Learned from the 2011 Great East Japan Earthquake, Tokyo, Japan, 1–4 March 2012; pp. 1398–1408.
56. Istrati, D.; Buckle, I. Role of Trapped Air on the Tsunami-Induced Transient Loads and Response of Coastal Bridges. *Geosciences* **2019**, *9*, 191. [[CrossRef](#)]
57. Higgins, C.C.; Lehrman, J.B.; Bradner, C.; Schumacher, T.; Cox, D.T. Hybrid testing of a prestressed girder bridge to resist wave forces. In Proceedings of the 29th US-Japan Bridge Engineering Workshop, Tsukuba, Japan, 7–9 November 2013; pp. 11–13.
58. Istrati, D.; Buckle, I.; Lomonaco, P.; Yim, S.; Itani, A. Large-scale Experiments of Tsunami Impact Forces on Bridges: The Role of Fluid-Structure Interaction and Air-Venting. In Proceedings of the 26th International Ocean and Polar Engineering Conference, Rhodes, Greece, 26 June–2 July 2016; pp. 761–768.

Disclaimer/Publisher’s Note: The statements, opinions and data contained in all publications are solely those of the individual author(s) and contributor(s) and not of MDPI and/or the editor(s). MDPI and/or the editor(s) disclaim responsibility for any injury to people or property resulting from any ideas, methods, instructions or products referred to in the content.